A Wearable Dual-Mode Repeater Antenna for Implant Communications

Kadircan Godeneli, Uzay Bengi, Omer A. Kati, and Sema Dumanli, *Member, IEEE*

***Abstract*—A novel wearable cavity-backed slot repeater antenna is presented to improve the link between implant antennas and the outside world. This proposed repeater antenna consists of two slots on opposite sides of a shallow rectangular cavity. These slots are activated in an alternating way, selecting the mode of operation: in-body or off-body. Through the antenna's in-body mode, signals transmitted by the implant antenna are received and conveyed to the off-body gateway via its off-body mode. Both modes are designed to operate in the 2.4 GHz Industrial, Scientific and Medical Band. The antenna is fed by a single diagonal stripline, and the two slots encounter the stripline at the same location with impedance matching obtained through offset feeding. The antenna has an overall size of 33.5 mm $\times$ 37 mm $\times$ 3.14 mm and has been shown to perform well near numerical and physical phantoms, communicating with deep tissue implants with an outstanding maximum $|S_{21}|$ value of -37.4 dB measured at 6 cm depth.**

***Index Terms*—Body sensor networks, implants, repeaters, slot antennas, wearable sensors, dual mode, two-mode repeater.**

I. Introduction

WIRELESS communication between implantable devices inside the human body and the outer world is a developing area as personalized healthcare draws increasing attention. Supporting preventive healthcare, implantable devices along with other on-body and off-body devices within the Body Area Network (BAN) are expected to decrease the medical costs, especially for patients with pre-existing medical conditions [1]. Communication between the implantable device and the BAN is generally established in the Medical Device Radiocommunications Service band (MedRadio) of 401–406 MHz or the Industrial, Scientific and Medical (ISM) radio bands of 2.4–2.5 GHz and 5.725–5.875 GHz [2]. However, one must note that communication through the human body requires extra care since the high water content of biological tissues leads to challenges in designing an in-body link [3]. The link suffers from reflections at the air and human body interfaces, as well as high propagation and near-field losses [4]. It is known that these limitations confine the in-body communication range for limited transmitter power. It should also be noted that the power transmitted by the implant antenna is restricted due to the battery lifetime of the device and the Specific Absorption Rate (SAR) limitations specified in the IEEE Standards [5]. In order to improve the connectivity, communication between an implant antenna and an off-body device can be split into multiple links using a repeater. An on-body repeater antenna can be used, allowing the implant antenna to communicate with the on-body repeater antenna, and then the repeater antenna communicates with the off-body station. This makes realizing reliable links possible with low transmit power levels, and enables low power implantable devices [6]. With the use of on-body repeater antennas, communication range can be extended, link reliability can be significantly improved, or the advantage can be translated into energy-saving to improve the battery lifetimes of the implants.

There are some examples of wearable repeater antennas in the literature [1], [3], [4], [6]–[15]. Many of them propose dual-band repeater antennas that use $401-406$ MHz and 2.4 GHz ISM band for in-body and off-body links, respectively [4], [6], [10]–[15]. However, the in-body link becomes more demanding in terms of data rate, which cannot be supported by the MedRadio band. Hence, repeater antennas operating at higher frequency bands for both in-body and off-body links are increasingly necessary, yet research is considerably weak on this topic [1], [3], [7]–[9]. In [8], [9], the operation frequencies are even higher than 2.45 GHz for the in-body link. This choice is suitable only for shallow implants since attenuation in human tissues increases with frequency. Therefore, their transmission performances cannot compete with repeaters operating at 2.45 GHz. Reference [3] chose 2.4 GHz ISM band for in-body and $4-10.6$ GHz band for off-body links. It has a relatively poor transmission performance compared to other 2.45 GHz in-body links. Moreover, the off-body frequency is in a higher band, leading to a large electrical size. This paper focuses on a solution where the 2.4 GHz ISM band is chosen for both in-body and off-body links. Reference [1] proposed using the 2.4 GHz ISM band for both links; however, two separate antennas were used for in-body and off-body links, which suggests a large on-body station. Reference [7] proposed an antenna with bi-directional radiation properties. The beam directed towards the human body is suitable for the in-body link, and the beam directed outwards is suitable for the off-body link. Although this proposal achieves optimum polarizations with a practical single feed structure, both modes are active simultaneously, which leaves the in-body link vulnerable to interference. Here, we propose a different approach and improve the in-body link's performance by at least 11 dB at an implant depth of 6 cm compared to the approach proposed in [7]. In our approach, the wearable repeater antenna has two separate modes: an in-body mode and an off-body mode, both operating in the 2.4 GHz ISM band. It is based on the authors' previous work [16] and patent [17], in which this concept was proposed for the

K. Godeneli, U. Bengi, O. A. Kati and S. Dumanli are with the Department of Electrical and Electronics Engineering, Boğaziçi University, İstanbul, 34343 Turkey e-mail: sema.dumanli@boun.edu.tr. This work was supported by Boğaziçi University Research Fund under project number 14543 and by TUBITAK 2247-A National Leader Researchers Award No. 120C131.

first time, but with only limited analysis and simulations. Here the idea is brought to a realistic environment with extensive analysis.

Since human tissues have no magnetic losses, high magnetic near fields are less susceptible to dissipation in the human body [18]. Thus, magnetic antennas, such as slot antennas, are better for facing the human body to communicate with an implant. Thus, in this study, the radiator for the in-body mode is chosen to be a slot. In order to create uni-directional radiation, this slot is backed with a shallow cavity and fed with a stripline feed. The off-body mode is also excited with the same stripline feeding another slot etched on the opposite facet of the cavity. The slots are activated in an alternating fashion, such that while one slot is active, the other is detuned via a shorting switch. In previous research, cavity-backed slot antennas have been shown to provide input impedance diversity [19] and polarization diversity [20] through multiple feeds before; on the other hand, radiation pattern diversity with a single feed has never been utilized prior to the present study.

A wearable antenna should either be flexible or small for user acceptability. Hence, in the proposed design, the upper slot responsible for off-body communications is meandered to achieve a small size for user acceptability [16]. A diagonal stripline is used, and the two slots intersect the stripline at the same location. Note that the vertical walls are realized using substrate integrated waveguides, namely a pin curtain structure. This has been shown to improve the repeatability of cavity-backed slot antennas [21].

A comparison between the proposed repeater antenna and closely related antennas in the literature can be seen in Fig. 1. The state-of-the-art is compared to the existing proposal in terms of essential aspects of the design, such as electrical size, antenna-human body separation (t_{air}), which is the gap between the repeater antenna and the muscle tissue, multimode operation, and operating frequency of the in-body mode. The comparison demonstrates the superior performance of the proposed antenna in many aspects.

This paper consists of 5 sections. The introduction is followed by Section II, where antenna design is presented. In Section III, the measurement setup is explained. Simulation and measurement results are discussed in Section IV. Finally, the work is concluded in Section V.

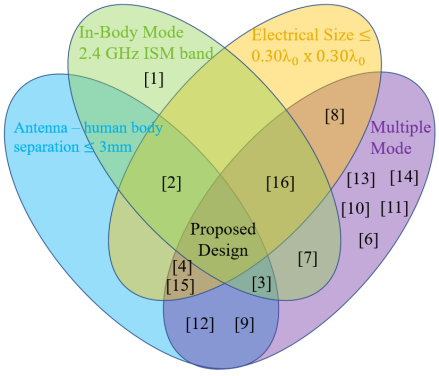

Fig. 1: A comparison between the proposed antenna and related antennas in the literature.

II. Antenna Design

The proposed repeater antenna has two slots on the opposite sides of a rectangular cavity, as seen in Fig. 2. The upper slot responsible for the off-body mode facing the air is meandered to achieve a small size for user acceptability with an overall size of 33.5 mm $\times$ 37 mm $\times$ 3.14 mm. Furthermore, it has a small electrical size ($0.27\lambda_0 \times 0.30\lambda_0$). The structure is realized with two layers of Rogers RT Duroid 5880 of $\epsilon_r = 2.2$ [22]. A single stripline connected to an SMA connector is sandwiched between the two substrates and feeds both slots. It is positioned diagonally, and the two slots encounter the stripline at the same location. The multimode operation is carried out in the 2.4 GHz ISM band for both in-body and off-body communications by detuning one slot with a switch while the other is active. It is envisaged that the repeater will control this switching operation digitally. Only one mode will be used at a time according to the mode of operation. In this way, radiation pattern diversity with two radiation modes will be achieved.

Given the target operating frequency and the relative permittivity of the substrate, the length of the upper slot facing the air can be calculated. Assuming a narrow and straight slot, the first order slot mode TE_{10} resonates when $L_{upper} = \frac{\lambda_{eff}}{2}, \lambda_{eff} = \frac{\lambda_0}{\sqrt{\epsilon_{r,eff}}}$, where λ_{eff} and $\epsilon_{r,eff}$ stand for effective wavelength and effective relative permittivity, respectively [23], [24]. Since the antenna's electric field is present both in the air and the substrate, $\epsilon_{r,eff}$ must be used in the calculations. For the upper slot, it can be calculated using

$$\epsilon_{r,eff} = \epsilon_{in} \cdot ff + \epsilon_{out} \cdot (1 - ff)$$

where ϵ_{in} and ϵ_{out} are the relative permittivity values of the media that the slot faces, 2.2 and 1, respectively, and ff stands for the filling factor. The typical filling factor for a cavity-backed slot antenna is known to be 10% [25], which has been validated here by numerical analysis through Ansys High Frequency Structure Simulator (HFSS) [26]. The calculated $\epsilon_{r,eff}$ is 1.12, which leads to an upper slot length of $L_{upper} = 5.78$ cm if the interaction of the slots is ignored. The length is further optimized through numerical analysis. The upper slot length is found to be 6.1 cm and 7.45 cm when the slot is straight and meandered, respectively. On the other hand, the analytical calculation of the lower slot length is more complicated since it faces several layers, including high permittivity muscle tissue; hence, the length is determined empirically. No further miniaturization is needed for the lower slot since the optimum length is 2.9 cm due to the human tissues' loading effect.

Note that during the analytical design of the slots, the interaction between the slots and the cavity is ignored. The backing cavity is shallow and intended to be non-resonant at the operating frequency to minimize this interaction. The cavity modes can be calculated using

$$f_{mnp} = \frac{c}{2\sqrt{\epsilon_r \mu_r}} \sqrt{\left(\frac{m}{a}\right)^2 + \left(\frac{n}{b}\right)^2 + \left(\frac{p}{h}\right)^2}$$

where a, b, h are cavity dimensions and m, n, p are mode numbers for a conventional cavity [27]. If the vertical walls

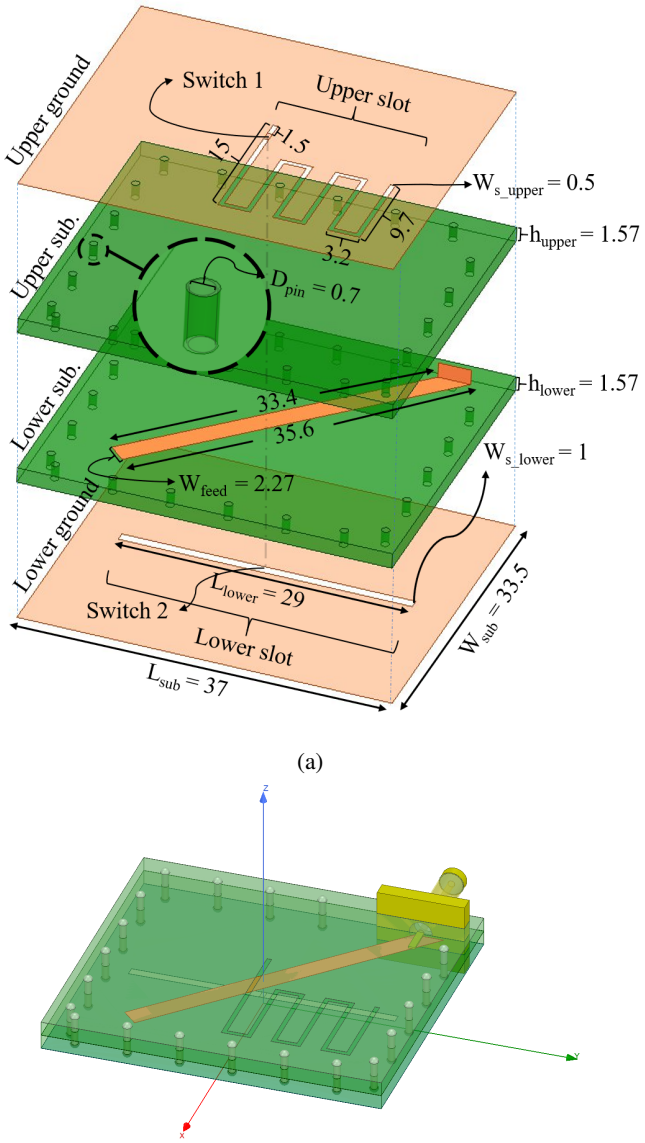

(a)

(b)

Fig. 2: The model of the proposed repeater antenna including the optimized dimensions. (a) Exploded view (units: mm). (b) Assembled model.

were perfect electrical conductors, the mode with the lowest resonant frequency, TE_{110}, would be expected to occur at 4.6 GHz. Here, the substrate integrated waveguide technique is applied instead of solid conducting walls. According to the previously studied guidelines [21], the pin diameter and spacing are determined to be 0.7 mm and 5 mm, respectively. The lowest resonant frequency mode is found to be 4.45 GHz through simulations when the effect of these vertical walls is taken into account, which assures that no cavity modes coincide with the fundamental slot modes.

Finally, the feed is optimized numerically. The feed offset and the feed length are the primary parameters affecting the matching. The stripline is located diagonally in the vertical mid-plane of the antenna. If both slots were facing identical mediums, a symmetrical structure with a central feed could provide impedance matching for each slot for a particular feed length. However, the loadings of the upper and lower slot here are different. Hence, the lower slot is first matched by optimizing the feed length with a central feed while the upper slot is deactivated. The upper slot is then moved in both directions to find the optimum feed offset for the upper slot while the lower slot remains deactivated. The designed antenna is prototyped using LPKF S103 [28], as seen in Fig. 3.

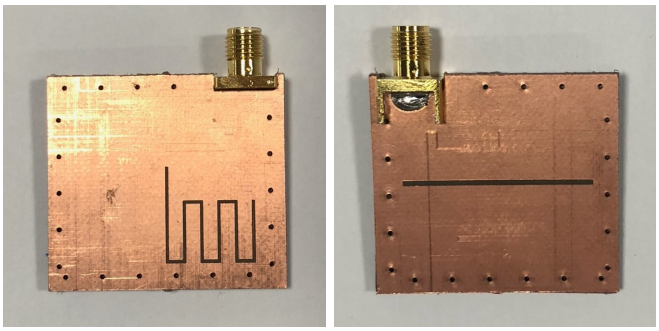

(a) (b)

Fig. 3: The top and the bottom views of the repeater antenna prototype. (a) Upper slot, off-body mode. (b) Lower slot, in-body mode.

In addition to the proposed repeater antenna, an implant patch antenna similar to [29] has been designed to evaluate the transmission performance. It is printed on Rogers RT/duroid 6006 having $\epsilon_r = 6.15$, a thickness of 1.91 mm and a size of 44.1 mm $\times$ 29.1 mm using LPKF S103. Furthermore, the rectangular patch has dimensions of 25 mm $\times$ 10 mm, and the feeding point is shifted by 10 mm from the center of the antenna. 1 mm spacing is introduced around the implant antenna to obtain an acceptable $|S_{11}|$ value at 2.45 GHz.

III. Measurement Setup

A physical chest phantom is developed using a hollow human model made of plastic. In order to create a more practical physical phantom, the area in which the measurements will be taken is separated from the rest of the structure, which is filled with isotonic (0.9%) water absorbed silica to minimize electromagnetic wave penetration. The measurements are conducted inside a polylactic acid (PLA) box filled with the muscle mimicking semi-liquid phantom. The inner dimensions of the box are 18 cm $\times$ 16 cm $\times$ 9.8 cm. The box and an elevator system controlling the implant antenna's depth are 3D printed and coated with a waterproofing spray. The box is then fixed inside the human model, as seen in Fig. 4. An RG402 coaxial cable is used to feed the implant antenna, and the calibration is performed at the end of the coaxial cable feeding the implant antenna [30]. Note that radiation due to the currents outside the coaxial cable is not expected since the implant antenna used in these measurements is not an electrically small antenna.

The muscle mimicking semi-liquid phantom in Fig. 4 (b) has been developed using the ingredients listed in Table

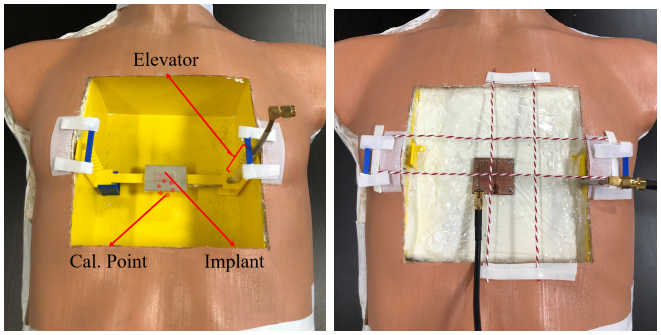

(a) (b)

Fig. 4: The physical chest phantom developed for the in-body measurements. (a) The 3D printed box and the elevator system fixed inside the human model. (b) The measurement box filled with the muscle mimicking semi-liquid phantom.

TABLE I
INGREDIENTS FOR A MUSCLE MIMICKING SEMI-LIQUID PHANTOM

Ingredient	Quantity
Deionized Water	2100 g
Oil	315 g
CTAB	until emulsified
Starch	450 g
Salt (NaCl)	20 g
Monopropylene glycol	20 ml

I. Cetyltrimethylammonium bromide (CTAB) is used as an emulsifying agent to mix the oil and the deionized water. Once homogeneity is achieved, starch is added, and the mixture is heated with a magnetic stirrer up to 60 °C for solidification. The permittivity of the mixture is measured as it cools down to room temperature. Note that the mixture's permittivity can be tuned for other tissues by changing the ratio of oil to water. Once the target permittivity is reached, salt is added to set the conductivity. Finally, monopropylene glycol is added as an antimicrobial agent. The relative permittivity and the conductivity of the developed muscle phantom are 48.6 and 2.13 S/m, respectively. Note that the target values at 2.4 GHz are 52.8 and 1.71 S/m [31]. Hence, the conductivity of the phantom used during the measurements is higher than the target value, and the link quality that the proposed antenna can provide is underestimated in these measurements.

IV. RESULTS AND DISCUSSION

A. Reflection Performance

Fig. 5 shows the simulated and measured reflection coefficient plots of each mode for $t_{air} = 1$ mm and 10 mm. The simulations include two different numerical phantoms: a single layer muscle phantom and Ansys male phantom (4 mm precision). The antenna model used for the simulations is a realistic model that includes an SMA connector and hemispheres mimicking soldering. In addition, each sheet is defined to have a thickness of 30 µm, and copper is used for conductors instead of perfect electric conductor. Fig. 5 (a), (b), (c), and (d) show the comparison of measured and simulated $|S_{11}|$ for both modes. It can be observed that the difference between the results generated with a single layer muscle phantom and Ansys male phantom is insignificant. For the sake of simplicity, a single layer muscle phantom is used for the rest of the paper. The in-body mode's matching deteriorates as the antenna is located closer to the human body; however, the off-body mode is immune to detuning. This is because the off-body mode is well isolated from the human body by the cavity. It can be observed that the measurements and simulations agree well in the off-body mode, whereas there is a disagreement in the in-body mode. Although both in-body and off-body modes are predicted by simulations to operate at 2.45 GHz, the in-body mode is measured to operate at 2.5 GHz due to the imperfect prototyping. The misalignment of the two substrates and the unintended air gap between them have been experimented with to cause repeatability issues. The effect of the unintended air gap (t_{air}^{sub}), the misalignment of the substrates (Δy_{sub}), and the mispositioning of the upper switch (Δx_{switch}) can be seen in Fig. 5 (e) where detuning is observed, supporting the repeatability issue regarding the discrepancies between measured and simulated in-body $|S_{11}|$ plots. The proposed structure would benefit from an automatized three-layered PCB printing process.

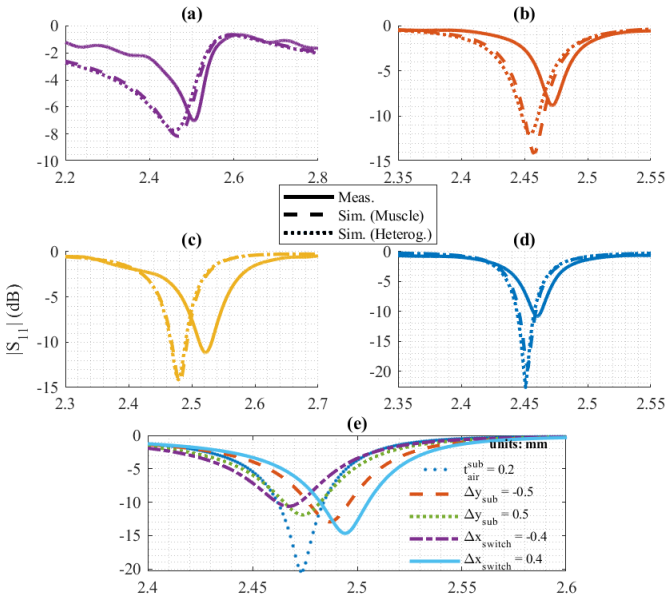

Fig. 5: Measured (solid lines) and simulated (dashed lines) $|S_{11}|$ (dB) for in-body and off-body modes of the repeater antenna for two different t_{air}: 1 mm and 10 mm. (a) In-body mode, $t_{air} = 1$ mm. (b) Off-body mode, $t_{air} = 1$ mm. (c) In-body mode, $t_{air} = 10$ mm. (d) Off-body mode, $t_{air} = 10$ mm. (e) Repeatability analysis for in-body mode, $t_{air} = 10$ mm.

B. Transmission Performance

The transmission performance of the in-body mode of the proposed repeater antenna and the effect of the t_{air} can be observed in Fig. 6 by plotting the Poynting vector fields at 2.45 GHz for an incident power of 10 mW. It should be noted that the presented data were first exported in 0.5 mm steps

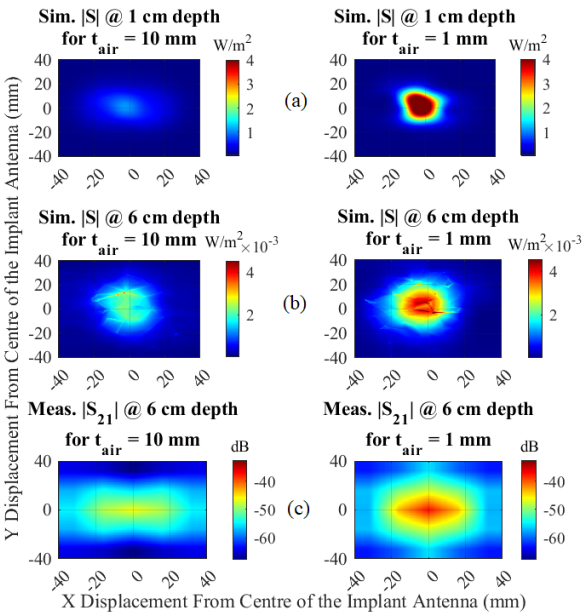

Fig. 6: The simulated Poynting vector magnitudes ($\mathrm{W/m^2}$) at (a) 1 cm and (b) 6 cm depths. (c) Measured $|S_{21}|$ (dB) grid at a depth of 6 cm for $t_{air} = 1$ mm and 10 mm.

and then interpolated. The time-averaged Poynting vector is integrated over a surface of 18 cm $\times$ 16 cm at 1 cm and 6 cm depths for $t_{air} = 1$ mm and 10 mm at 2.45 GHz. At 1 cm depth, the surface integral values of 2.30 mW and 1.12 mW are computed for $t_{air} = 1$ mm and 10 mm, respectively, whereas that of 5.32 µW and 3.71 µW are obtained at 6 cm depth.

Moreover, to validate the simulated Poynting vector plots, a grid of measurements has been taken in a quadrant. The grid of points are separated by 2 cm steps in both x and y directions. The results are interpolated, as seen in Fig. 6 (c). An implant patch antenna is used for these analyses, and an agreement with the simulations has been observed. Hence, a 1 mm separation that provides superior performance and better user acceptance is chosen.

Transmission performance of the in-body mode for $t_{air} = 1$ mm is evaluated through simulations and measurements of the transmission coefficient. The implant antenna's depth is changed from 2 cm to 6 cm. $|S_{21}|$ plots for various depths and t_{air} values can be seen in Fig. 7. The agreement between the measurements and simulations is remarkable. Note that the wide bandwidth of the implant antenna causes a flatter $|S_{21}|$ response in the 2.4 GHz ISM band.

In order to present the advantage of using two modes, the transmission coefficient when communicating with the implant antenna at 6 cm depth is simulated and measured for both in-body and off-body modes, as seen in Fig. 8. If a single-mode repeater antenna were used, instead of two modes, the transmission would be 5.2 dB worse for $t_{air} = 1$ mm.

Finally, to demonstrate the effect of using a repeater antenna on the battery lifetime of the implant, the transmission coefficient between the implant and an off-body gateway, which is only 55 cm away from the human body, is measured. Fig. 9 presents the link between the off-body mode and off-body gateway, completing the full picture of the repeater antenna's transmission scenario. As seen in Fig. 9, the in-body mode of the proposed repeater antenna significantly improves the $|S_{21}|$ value when compared to the link without the repeater antenna. If the implant were to communicate with the off-body station directly, $|S_{21}|$ would be -62.6 dB. On the other hand, if the implant communicates with the proposed repeater antenna, $|S_{21}|$ is -37.4 dB. Assuming the same sensitivity

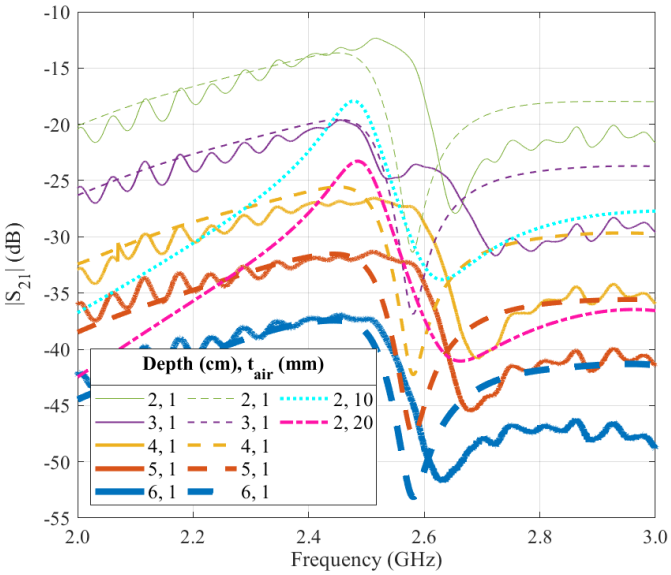

Fig. 7: Simulated (dashed lines) and measured (solid lines) transmission coefficients between the in-body mode of the repeater and the implant for different implant depths (2, 3, 4, 5, 6 cm), and t_{air} (1, 10 and 20 mm).

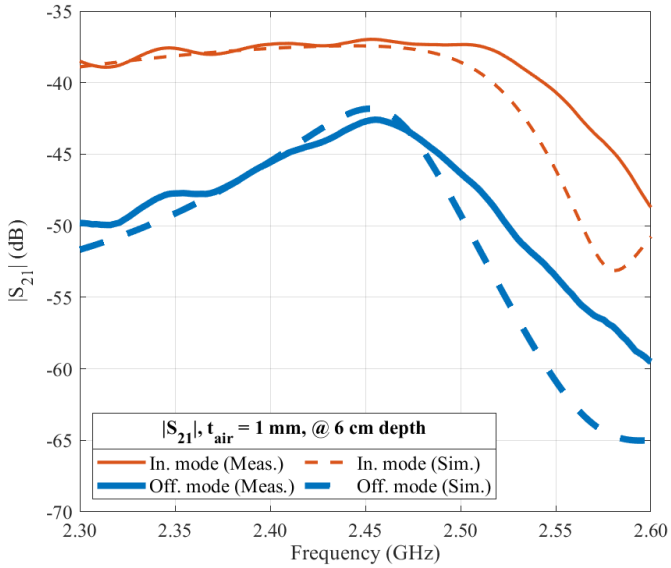

Fig. 8: Simulated and measured transmission coefficients between the implant and the in-body and off-body modes while the implant antenna is at 6 cm depth for $t_{air} = 1$ mm.

for the repeater and the off-body gateway, the implant should transmit 25.2 dB more power to establish a reliable link with the off-body gateway without the use of a repeater antenna for $t_{air} = 1$ mm. Hence, the repeater antenna allows an extended lifetime for the implant antenna. The superior performance of 1 mm separation over 1 cm separation can also be observed.

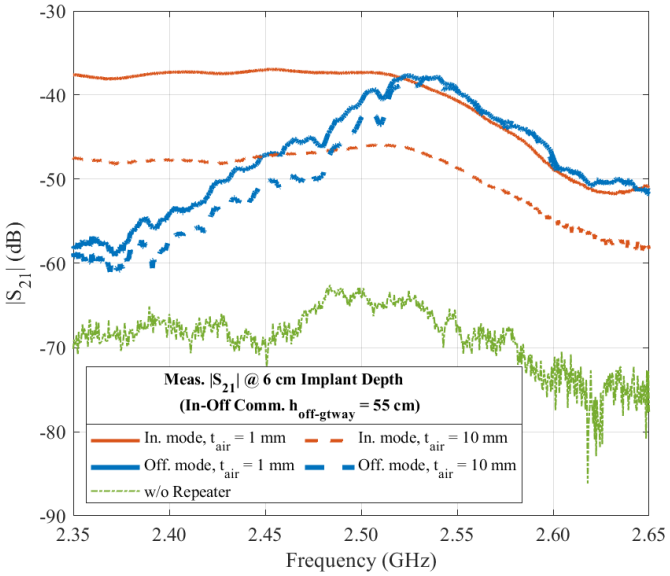

Fig. 9: Measured transmission coefficients between the in-body mode and the implant, the off-body mode and an off-body gateway, and the implant and the off-body gateway representing the direct link without the repeater.

Table II provides a detailed comparison of the wearable repeater antennas in the literature in terms of operating frequency, antenna-human body separation, and size. The proposed design operates at 2.45 GHz for both in-body and off-body modes, which is a substantial improvement in data rate for implant communications. User acceptability is achieved with a small physical size, in addition to 1 mm of separation between the repeater and the human body. In addition, the proposed repeater antenna has one of the smallest electrical sizes compared to other designs. To make the comparison more quantitative, Table III is generated to show transmission performances. Estimated $|S_{21}|$ values at 60 mm depth for each design can be seen in Table III, aiming to make a like-for-like comparison. Note that different implant antennas might have been used in these proposals. However, because the efficiencies of these implant antennas are generally low, the effect of this variation can be ignored. Within this scope, in [7], estimated $|S_{21}|$ values at 75 mm depth were calculated since one cannot compare $|S_{21}|$ values at different depths. Likewise, attenuation (α) is calculated using

$$\alpha = (Ae^{B\epsilon_r} + D) \cdot (E\sigma + F)$$

where the constants A, B, D, E and F are 3.02, -0.04, 1.83, 0.11 and 0.07, respectively, and ϵ_r and σ are the relative permittivity and conductivity of the phantom [32]. Note that the attenuation is converted to dB/cm. Estimated $|S_{21}|$ values are obtained at 60 mm depth for each design. It is seen that our proposal proves to be a superior design with $|S_{21}| = -37.4$ dB at 60 mm depth compared to other designs in the literature. Note that there are two $|S_{21}|$ values indicated in Table III for this research, the first for the muscle phantom with $\epsilon_r = 48.6$ and $\sigma = 2.13\,\mathrm{S/m}$, and the second with $\epsilon_r = 52.8$ and $\sigma = 1.71\,\mathrm{S/m}$. The first set is the electrical properties of the physical phantom that was developed. Due to the large size of the phantom, any further fine-tuning was not possible at the time. This first set is also used for the numerical phantom throughout the paper. However, the target properties of the muscle at 2.4 GHz is the latter set, and since the conductivity is lower, the transmission performance is expected to be even better. The expected $|S_{21}|$ value of -31 dB for the latter case is provided as an indicator of the antenna's real-life performance. Compared to a closely related antenna [7], which has an estimated maximum $|S_{21}|$ value of -48.62 dB, here an 11 dB improvement is achieved at 6 cm implant depth. Since this improvement is measured using a high conductivity muscle phantom, it is expected to be 17 dB in a real-life scenario, as predicted in Table III. Although the proposed repeater antenna suffers from higher path loss due to operation at 2.45 GHz rather than 0.4 GHz and communication through more conductive muscle tissue compared to most of the related antennas in the literature, it achieves a superior transmission performance. All in all, the proposed design is the only model having an electrical size smaller than $0.30\lambda_0 \times 0.30\lambda_0$, separation less than 3 mm, multimode operation through switching, $|S_{21}|$ greater than -40 dB, and high data rate (2.45 GHz compared to 400 MHz) for in-body communications.

Fig. 10 (a) shows the 2D directivity pattern of the off-body mode at $\phi = 0°$ and $\phi = 90°$ planes for $t_{air} = 1$ mm and Fig. 10 (b) shows the 3D radiation patterns. The 2D pattern is measured in an open area. Before the measurements, the ambient electromagnetic noise within the area is checked using an Electromagnetic Field Strength Meter to ensure no interference. The electric field is measured to be lower than the threshold value of 0.3 V/m between 0.1 MHz to 3000 MHz. The 3D radiation patterns are measured in a 2.43 m x 2.43 m x 2.40 m anechoic chamber by Rohde & Schwarz (OTA Performance Test System WPTC-XS). It can be seen that the simulations agree with the measurements. The pattern is directional, which is expected and suitable to establish an off-body link. The maximum gain at 2.45 GHz for the off-body mode is 0.58 dB and 2.8 dB for $t_{air} = 1$ mm and 10 mm, respectively. The off-body mode's efficiency is simulated to be 27% and 36% for $t_{air} = 1$ mm and 10 mm, respectively. The efficiency decreases with decreasing t_{air} due to increasing near field losses, as the fields are confined more in the lossy medium. Moreover, SAR of the antenna is simulated on the surface of the numerical phantom at the frequency where the minimum of $|S_{11}|$ occurs for in-body and off-body modes. 1 g average SAR for an incident power of 10 mW, when $t_{air} = 1$ mm, is 1.32 W/kg and 1.20 W/kg for the in-body and off-body modes, respectively, whereas it is 0.18 W/kg and 0.15 W/kg for $t_{air} = 10$ mm, abiding by the limit of 2 W/kg set in the European Standards.

TABLE II
COMPARISON OF SOME PROPERTIES BETWEEN ANTENNAS IN THE LITERATURE AND THE PROPOSED ANTENNA

Ref	In-body freq. (GHz)	On/Off-body freq. (GHz)	Separation (mm)	Dimensions (mm)	Electrical Size
[1]	2.45	-	7.92	$40.9 \times 48.7 \times 3.94$	$0.33\lambda_0 \times 0.40\lambda_0$
[2]		-	0	$22 \times 22 \times 10$	$0.18\lambda_0 \times 0.18\lambda_0$
[3]		$4 - 10.6$		$\pi \times 17.5^2 \times 0.76$	$\pi \times 0.23^2\lambda_0^2$ - $\pi \times 0.62^2\lambda_0^2$
[4]	0.4	2.45		$26.8 \times 28 \times 0.635$	$0.22\lambda_0 \times 0.23\lambda_0$
[6]			15	$60 \times 70 \times 1.6$	$0.49\lambda_0 \times 0.57\lambda_0$
[7]	2.45		5	$67 \times 31 \times 8.9$	$0.55\lambda_0 \times 0.25\lambda_0$
[8]	5.8		10	$28 \times 15.5 \times 10.5$	$0.23\lambda_0 \times 0.13\lambda_0$
[9]	3.5–4.5	5.8	3	$40 \times 20 \times 0.762$	$0.77\lambda_0 \times 0.39\lambda_0$
[10]	0.4	2.45	5	$40 \times 40 \times 3.2$	$0.33\lambda_0 \times 0.33\lambda_0$
[11]	0.4, 1.4		10	$40 \times 40 \times 1.6$	$0.33\lambda_0 \times 0.33\lambda_0$
[12]	0.4		0	$76 \times 67 \times 1.5$	$0.62\lambda_0 \times 0.55\lambda_0$
[13]			10	$40 \times 40 \times 1.6$	$0.33\lambda_0 \times 0.33\lambda_0$
[14]			5	$\pi \times 28^2 \times 4.8$	$\pi \times 0.23^2\lambda_0^2$
[15]			0	$19.2 \times 6.5 \times 0.6$	$0.16\lambda_0 \times 0.05\lambda_0$
[16]	2.45		40	$30 \times 30 \times 3.15$	$0.25\lambda_0 \times 0.25\lambda_0$
This work	2.45		1	$33.5 \times 37 \times 3.14$	$0.27\lambda_0 \times 0.30\lambda_0$

TABLE III
TRANSMISSION PERFORMANCES OF REPEATER ANTENNAS IN THE LITERATURE AND THE PROPOSED ANTENNA

Ref	Depth (mm)	Tissue	Peak $\lvert S_{21}\rvert$ (dB)	Attenuation (dB/cm)	Est. $\lvert S_{21}\rvert$ @ 60 mm (dB)
[3]	30	Muscle	-37	4.92	-51.76
[4]	9	Muscle	-24	2.93	-38.94
[6]	10	Muscle	-50	2.93	-64.65
[7]	75	Muscle	-56	4.92	-48.62
[8]	5	Muscle	-26	12.11	-92.61
[9]	5	Bone	-16.8	4.98	-44.19
This work	60	Muscle	-37.4 / -31	5.98 / 4.92	-37.4 / -31

V. CONCLUSION

This article discussed a novel wearable cavity-backed slot repeater antenna with a multimode operation, both in the 2.4 GHz ISM band, that switches between these two modes, thus providing radiation pattern diversity. These modes constitute in-body and off-body links for the repeater antenna, which communicate respectively with an implant antenna and an off-body station. The proposed design has been shown to have a superior transmission performance compared to similar antennas in the literature. The model was simulated using a numerical phantom, and these results have been verified via measurements on a physical phantom. It has been shown that the proposed repeater antenna significantly improves the battery lifetime of the implant when compared to direct communication between the implant antenna and the off-body station. The implant's transmit power level can be reduced since the $|S_{21}|$ value is -37.4 dB for the in-body mode of the repeater antenna, whereas $|S_{21}|$ value is -62.6 dB for an off-body patch antenna 55 cm away from the human tissue, both communicating with the implant antenna at 6 cm depth. It has also been shown that the use of two modes is more advantageous than a single-mode repeater antenna by comparing the links in-body and off-body modes form when communicating with an implant antenna. In the future, the effect of using a dual-mode antenna on communication system performance can be investigated through channel measurements.

ACKNOWLEDGMENT

The authors would like to thank Arçelik Inc. and Murat Can Akçay, Ozan Furkan Sezgen, and Onur Tatar for their support in measurements.

REFERENCES

[1] S. Agneessens, P. Van Torre, E. Tanghe, G. Vermeeren, W. Joseph, and H. Rogier, "On-body wearable repeater as a data link relay for in-body wireless implants," *IEEE Antennas and Wireless Propagation Letters*, vol. 11, pp. 1714–1717, 2012.

[2] J. Blauert and A. Kiourti, "Bio-matched horn: A novel 1–9 GHz on-body antenna for low-loss biomedical telemetry with implants," *IEEE Transactions on Antennas and Propagation*, vol. 67, no. 8, pp. 5054–5062, 2018.

[3] J. M. Felício, J. R. Costa, and C. A. Fernandes, "Dual-band skin-adhesive repeater antenna for continuous body signals monitoring," *IEEE Journal of Electromagnetics, RF and Microwaves in Medicine and Biology*, vol. 2, no. 1, pp. 25–32, 2018.

[4] L.-J. Xu, Z. Duan, Y.-M. Tang, and M. Zhang, "A dual-band on-body repeater antenna for body sensor network," *IEEE Antennas and Wireless Propagation Letters*, vol. 15, pp. 1649–1652, 2016.

[5] IEEE Standard for Safety Levels with Respect to Human Exposure to Radio Frequency Electromagnetic Fields, 3 kHz to 300 GHz, IEEE Standard C95.1, 2019.

[6] A. Kiourti, J. R. Costa, C. A. Fernandes, and K. S. Nikita, "A broad-band implantable and a dual-band on-body repeater antenna: Design and transmission performance," *IEEE Transactions on Antennas and Propagation*, vol. 62, no. 6, pp. 2899–2908, 2014.

[7] M. K. Magill, G. A. Conway, and W. G. Scanlon, "Circularly polarized dual-mode wearable implant repeater antenna with enhanced into-body gain," *IEEE Transactions on Antennas and Propagation*, vol. 68, no. 5, pp. 3515–3524, 2020.

[8] J. Tak, K. Kwon, S. Kim, and J. Choi, "Dual-band on-body repeater antenna for in-on-on WBAN applications," *International Journal of Antennas and Propagation*, vol. 2013, 2013.

[9] Z. Duan, L.-J. Xu, and W. Geyi, "Metal frame repeater antenna with partial slotted ground for bandwidth enhancement of wristband devices," *IET Microwaves, Antennas & Propagation*, vol. 11, no. 10, pp. 1438–1444, 2017.

[10] K. Kwon, J. Tak, and J. Choi, "Design of a dual-band antenna for wearable wireless body area network repeater systems," in *2013 7th European Conference on Antennas and Propagation (EuCAP)*, pp. 418–421, IEEE, 2013.

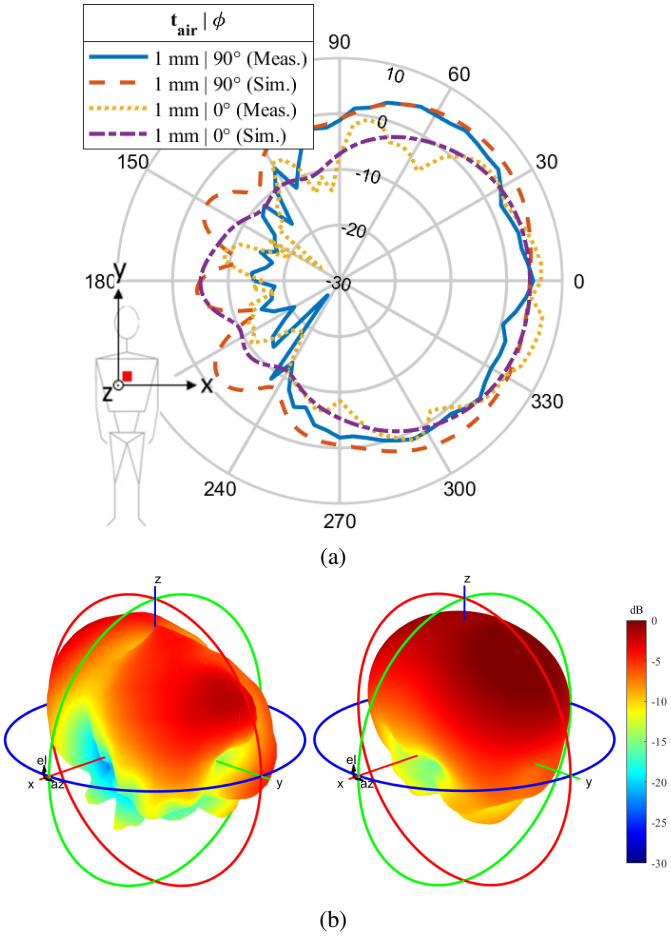

Fig. 10: Simulated and measured radiation patterns of the off-body mode with $t_{air} = 1$ mm. (a) 2D plots for $\phi = 0°$ and $90°$. (b) 3D polar plots (measurement: left, simulation: right).

[11] K. Kwon, J. Tak, and J. Choi, "Design of a triple-band on-body antenna for a biomedical repeater application," in *2013 IEEE Antennas and Propagation Society International Symposium (APSURSI)*, pp. 2093–2094, IEEE, 2013.

[12] M. S. Miah, C. Icheln, and K. Haneda, "A dual-band repeater antenna for on-body receiver unit of wireless capsule endoscope," in *2020 14th European Conference on Antennas and Propagation (EuCAP)*, pp. 1–4, IEEE, 2020.

[13] K. Kwon, J. Tak, and J. Choi, "Design of a dual-band on-body antenna for a wireless medical repeater system," *The Journal of Korean Institute of Electromagnetic Engineering and Science*, vol. 24, no. 3, pp. 239–246, 2013.

[14] X. Tong, C. Liu, H. Guo, and X. Liu, "A triple-mode reconfigurable wearable repeater antenna for WBAN applications," *International Journal of RF and Microwave Computer-Aided Engineering*, vol. 29, no. 3, p. e21615, 2019.

[15] L.-J. Xu, Z. Duan, and Y. Bo, "Compact spiral antenna for dual-band on-body applications," in *2017 International Applied Computational Electromagnetics Society Symposium (ACES)*, pp. 1–2, IEEE, 2017.

[16] S. Dumanli, "A digitally assisted repeater antenna for implant communications," in *2017 11th European Conference on Antennas and Propagation (EUCAP)*, pp. 181–184, IEEE, 2017.

[17] S. Dumanli Oktar, "Relay device for relaying radio frequency signals received from an antenna implanted within a patient's body to another device," Dec. 11 2018. US Patent 10,149,636.

[18] F. Merli, B. Fuchs, J. R. Mosig, and A. K. Skrivervik, "The effect of insulating layers on the performance of implanted antennas," *IEEE Transactions on Antennas and Propagation*, vol. 59, no. 1, pp. 21–31, 2010.

[19] J. S. Lee, S. J. Kim, S. J. Yun, S. W. Nam, and S. M. Yun, "2-port antenna having optimum impedances of a transmitter and a receiver," Aug. 1 2017. US Patent 9,722,317.

[20] Y. Dong and T. Itoh, "Miniaturized cavity-backed dual-polarized slot antenna," in *Proceedings of the 2012 IEEE International Symposium on Antennas and Propagation*, pp. 1–2, IEEE, 2012.

[21] S. Dumanli, C. J. Railton, D. L. Paul, and G. S. Hilton, "Closely spaced array of cavity backed slot antennas with pin curtains walls," *IET Microwaves, Antennas & Propagation*, vol. 5, no. 1, pp. 38–47, 2011.

[22] Rogers Corporation. Accessed: Jan. 2021. [Online]. Available: https://www.rogerscorp.com/advanced-connectivity-solutions.

[23] C. A. Balanis, *Antenna theory: analysis and design*. John Wiley & Sons, 2016.

[24] E. Cil and S. Dumanli, "The design of a reconfigurable slot antenna printed on glass for wearable applications," *IEEE Access*, vol. 8, pp. 95417–95423, 2020.

[25] S. Dumanli, C. J. Railton, and D. L. Paul, "A slot antenna array with low mutual coupling for use on small mobile terminals," *IEEE Transactions on Antennas and Propagation*, vol. 59, no. 5, pp. 1512–1520, 2011.

[26] ANSYS HFSS: High Frequency Electromagnetic Field Simulation Software. Accessed: Oct. 2020. [Online]. Available: https://www.ansys.com/products/electronics/ansys-hfss.

[27] D. M. Pozar, *Microwave engineering*. John Wiley & Sons, 2011.

[28] LPKF S103. Accessed: Jan. 2021. [Online]. Available: https://www.lpkfusa.com/datasheets/prototyping/s103.pdf.

[29] M. Mokhtar, K. Kamardin, Y. Yamada, R. H. M. Baharin, N. H. Abd Rahman, N. Zainudin, T. A. Latef, and M. N. M. Yasin, "Implantable patch antenna for body communication," in *2018 2nd International Conference on Telematics and Future Generation Networks (TAFGEN)*, pp. 77–80, IEEE, 2018.

[30] Y. El-Saboni, M. K. Magill, G. A. Conway, S. L. Cotton, and W. G. Scanlon, "Measurement of deep tissue implanted antenna efficiency using a reverberation chamber," *IEEE Journal of Electromagnetics, RF and Microwaves in Medicine and Biology*, vol. 1, no. 2, pp. 90–97, 2017.

[31] IT'IS foundation dielectric properties database. Accessed: Sept. 2020. [Online]. Available: https://itis.swiss/virtual-population/tissue-properties/database/dielectric-properties/.

[32] D. Kurup, W. Joseph, G. Vermeeren, and L. Martens, "In-body path loss model for homogeneous human tissues," *IEEE Transactions on Electromagnetic Compatibility*, vol. 54, no. 3, pp. 556–564, 2011.

Kadircan Godeneli received the B.Sc. degrees in both electrical and electronics engineering and physics from Boğaziçi University, Istanbul, Turkey, in 2021. He was an exchange student at the Nanyang Technological University, Singapore in Spring 2020. He is currently a Ph.D. student in the Department of Electrical Engineering and Computer Sciences at the University of California, Berkeley.

His research interests lie at the intersection of electrical engineering and physics, including quantum devices based on superconducting qubits.

Uzay Bengi received the B.Sc. degree in electrical and electronics engineering from Boğaziçi University, Istanbul, Turkey, in 2020 and currently is an M.Sc. student at Boğaziçi University.

He has been a researcher at the Antennas & Propagation Laboratory (BOUNtenna) since 2019 and working as a teaching assistant at Istanbul University-Cerrahpasa, Istanbul, Turkey since 2021. His current research covers antenna design for body area networks, wearable wireless monitoring systems and implantable devices.

Omer A. Kati is currently studying electrical and electronics engineering at Boğaziçi University, Istanbul, Turkey. He was an erasmus student at Poznan University of Technology (PUT), Poland in Spring 2021.

He is currently a member of the Antennas & Propagation Research Laboratory (BOUNtenna). His current research interests include machine learning and its applications in wearable antenna design and implant communications.

Sema Dumanli (M'11) received the Bachelors degree in electrical and electronic engineering from Orta Doğu Teknik Üniversitesi, Ankara, Turkey, in 2006 and the Ph.D. degree from the University of Bristol, Bristol, U.K., in 2010.

She was with Toshiba Research Europe, Bristol, as a Research Engineer and a Senior Research Engineer from 2010 to 2017. She is currently an Assistant Professor with Boğaziçi University, Istanbul, Turkey. Her current research interests include antenna design for body area networks, implantable and wearable devices, eHealth, and multiscale communications.